GeoScienceWorld
Lithosphere
Volume 2022, Article ID 2520477, 18 pages
https://doi.org/10.2113/2022/2520477

Lithosphere

Research Article

Movement Law of Overlying Strata and Abutment Pressure Redistribution Characteristic Based on Rigid Block

Fang Yuan,[1,2] **Jianxin Tang**,[1,2] **and Lingrui Kong**[1,2]

[1]*State Key Laboratory of Coal Mine Disaster Dynamics and Control, Chongqing University, Chongqing 400044, China*
[2]*School of Resources and Safety Engineering, Chongqing University, Chongqing 400044, China*

Correspondence should be addressed to Fang Yuan; 348329045@qq.com, Jianxin Tang; jxtang@cqu.edu.cn, and Lingrui Kong; 877986848@qq.com

Received 15 June 2022; Revised 30 November 2022; Accepted 15 December 2022; Published 31 December 2022

Academic Editor: Songjian Ao

Roof movement induced by coal excavation is the immediate cause of rock pressure redistribution and strata behavior. The rigid block in PFC3D was used to generate a multijointed rock mass, and the PFC3D–FLAC3D coupling model was used to study the movement law of the highly developed structural plane of the overlying strata. Strata movement and abutment pressure redistribution characteristics were obtained. The numerical simulation results showed that the multijointed rock mass model reproduced a rock mass with highly developed structural planes. After coal seam mining, the immediate roof caved and filled the goaf, forming an irregular and regular caved zone. The immediate roof shear slipped along the coal wall. The fracture of the basic roof formed a fractured zone, and the maximum height of the fractured zone first increased and then decreased, exhibiting continuous slow subsidence. The fluctuation of the front abutment pressure was reduced, and the abutment pressure in the goaf jumps was discontinuous. The abutment pressure in the goaf was high in the middle and low on both sides. After the initial fracture of the basic roof, the stress concentration of some rock blocks in the goaf exceeded the in-situ stress, and the average abutment pressure increased with the working face advancing length. With the coal wall of the working face gradually moving away from the goaf, the abutment pressure of the goaf first increased and then remained unchanged; the porosity first decreased sharply and then declined slowly; the coordination number of particles rose sharply and then increased slowly, indicating that the goaf gradually stabilized. Similar simulation results indicated that the variation law of abutment pressure, caving characteristics of the immediate roof, and continuous slow subsidence of the basic roof were the same as those of the numerical simulation.

1. Introduction

The overlying strata movement induced by coal seam mining is the leading cause of mining accidents. Therefore, mastering the movement laws of overlying strata has become an essential requirement for mining safety. Field practice indicates that under the conditions of the strike-retreating longwall mining and natural cave methods, the goaf behind the working face can usually be divided into three zones along the vertical direction: caved, fractured, and bending subsidence zones (Figure 1(b)) [1, 2]. Owing to the difference in roof lithology and caving height, the immediate roof usually fills the goaf with rock blocks to form a caved zone (Figures 1(a), 1(c), and 1(d)); the bulking factor is usually 1.3–1.5 [3]. The basic roof is usually fractured with a plate and generates fractures to form a voussoir beam structure, known as a fractured zone [4, 5]. The overlying strata on the basic roof continuously sink, creating a bending subsidence zone. Owing to the concealment of underground mining engineering, determining the movement law of the field overlying strata using existing technical methods is difficult. Therefore, studying the movement law of the overlying strata and reproducing the development characteristics of the three zones through numerical simulations are essential. In the Xuyong mining area of Sichuan Province, China, the coal-bearing measure (Permian System Longtan Formation) is dominated by sandy mudstone with low rock mass strength and developed structural planes. Considering the

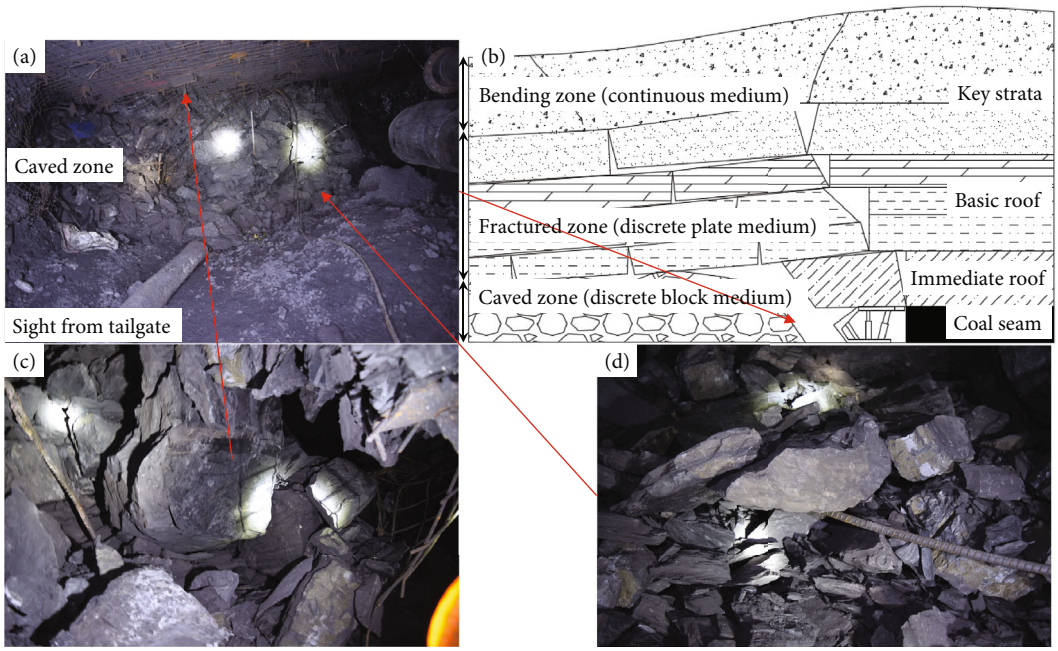

Figure 1: Characteristics of three zones of a mining field.

lack of effective research methods, few studies have been conducted on the movement law of soft strata on developed structural planes, leading to uncertainties regarding the mechanisms of roof accidents in the soft strata of the working faces of thin coal seams, inhibiting the development of prevention and control measures.

According to rock pressure theory [1, 6] and the morphology of a caved zone (Figure 1), the caved zone comprises discrete rock blocks, the fractured zone comprises discrete rock plates, and the bending subsidence zone is similar to a continuum medium. The FLAC3D software, based on the finite difference method (FDM), has been used to simulate the continuum subsidence of overlying strata after coal seam mining and has achieved many beneficial results [7–10]. The FDM is useful in the continuous deformation of a rock mass but does not conform to the separation, fracture, subsidence, collapse, and accumulation characteristics of the two zones (caved and fractured zones). PFC3D software, based on the discrete element method (DEM), can simulate the motion of a discrete medium, but its low computational efficiency limits its applicability. Developing the DEM–FDM coupling theory [11–14] and updating the PFC3D–FLAC3D coupling numerical simulation technology [15–17] enables the use of the PFC3D–FLAC3D coupling method to study the movement law of highly developed structural plane overlying strata. This method has the advantages of PFC3D for simulating the movement of a discrete medium and the high computational efficiency of FLAC3D. Although the PFC3D–FLAC3D coupling numerical simulation method has excellent application prospects in mining engineering, few reports have examined these prospects.

The PFC3D provided a reference example for simulating the uniaxial compression of rock specimens. It showed that the Rigid block assembly could simulate the mechanical behavior of rock, such as elasticity, fracture, and postpeak softening. Tan et al. [18] used the Rigid block assembly to simulate the deformation characteristics of geotextile-encased stone columns under uniaxial compression and verified with experiments. Li et al. [19] and Li et al. [20] used the clump element to study the compressive deformation characteristics of goaf materials. Yuan et al. [21] also used the clump element to study the compressive deformation characteristics of goaf materials and verified by field tests. Rigid block is a simplified unit of the clump, indicating that the Rigid block assembly can effectively simulate the mechanical behavior of the goaf materials. However, few studies used Rigid blocks to simulate the movement law of overlying strata. This paper based on the results of field investigation, that the characteristics of goaf gangue caving and the fragmentation degree of the core, it is considered that there are a large number of joints, fissures, and stratification in a weak rock mass. Therefore, the Rigid block was used to generate the stratum and simulate the primary joint in a weak rock mass.

This study analyzed the rock mass structure of soft rocks in the Xuyong mining area. The PFC3D–FLAC3D coupling numerical simulation method was used to establish a two-dimensional plane strain model along the strike direction in the middle of a working face to study the movement law of multijointed overlying strata and the redistribution characteristics of the abutment pressure. This method was verified using a similar simulation test.

2. Numerical Simulation

2.1. Engineering Overview. Xuyong No.1 coal mine, located in Zhengdong Town, Xuyong County, Sichuan Province, China, was considered the engineering background for this study. The coal-bearing strata in the mining area include

No.	Lithology	Geological formations	Thickness (m)	Depth (m)
1	Sandy mudstone		9.7	180.8
2	Sandy mudstone		13.4	190.5
3	Changing limestone		41.3	203.8
4	Sandy mudstone		12.1	247.4
5	Clay		3.1	259.5
6	Sandy mudstone		2.8	262.6
7	Sandy mudstone		6.6	265.4
8	Siltstone		3.1	272.0
9	Sandy mudstone		0.6	275.1
10	Sandy mudstone		32.0	275.7
11	Sandy mudstone		1.7	307.7
12	Sandy mudstone		5.3	309.4
13	Coal seam C_{19}		0.9	314.7
14	Sandy mudstone		2.7	315.6
15	Coal seam C_{20}		1.0	318.3
16	Sandy mudstone		8.0	319.3
17	Siltstone		3.6	327.4
18	Sandy mudstone		0.3	330.9
19	Coal seam C_{24}		1.1	331.2
20	Sandy mudstone		0.7	332.3

(a)

(b)

(c)

Figure 2: Borehole columnar section and core.

the Longtan Formation of the upper Permian. The average thickness of coal seam C_{19} is 1.0 m, and the average mining height is 1.5 m. The working face was mined using the strike-retreating longwall mining method, and the goaf was managed using the natural caving method. According to the borehole columnar section (Figure 2(a)), the coal seam roof is mainly sandy mudstone, and the average uniaxial compressive strength is approximately 20 MPa, indicating soft rock. Simultaneously, core drilling in the area without mining disturbance indicates that there are few cores with a length of more than 10 cm (Figures 2(b) and 2(c)), with most cores broken into granules, indicating that the stratification, joints, and fissures are developed in the overlying strata of the mining face, and the rock mass structural plane has "rich joints." These analyses indicate that the roof is a soft and multijointed rock mass.

According to field observations, the immediate roof caved along with the coal excavation and filled the goaf. Therefore, the thickness of a single layer can be considered as 1 m. The basic roof's first weighting step distance was 24.5 m, and the average periodic weighting step distance was 12.3 m (Figure 3). The average tensile strength of sandy mudstone is 5.0 MPa, and the volumetric weight is 30.0 kN/m^3. When the thickness of the basic roof was 2 m, the initial and periodic fracture step distances were calculated according to the fixed and cantilever beams in the mechanics of materials. They were 25.8 m and 10.5 m, respectively, similar to the field observation results of rock pressure.

2.2. Modeling. Soft rocks, such as sandy mudstone, are caused by the low strength of the rock block itself and cutting by the structural plane, compromising the integrity of the rock mass. Therefore, according to the structural characteristics of the rock block in the caved zone (Figure 1) and core integrity (Figures 2(b) and 2(c)), the rock blocks formed by structural plane cutting in the soft and multijointed rock mass were simplified as tetrahedral elements, and the rigid block (Rblock) in PFC3D was used to generate the original strata model. The rigid block module introduced the capability of modeling closed, convex, and manifolds that are polyhedra in PFC3D. The facets of the rigid blocks were triangles. The rigid blocks in the model domain can interact with the balls, clumps, walls, zones, and structural elements. They can be created from vertices, imported from geometric objects, and cut and support the edge/vertex rounding.

In FLAC3D and PFC3D, computational and plotting engines are designed as plug-ins for a common graphical user interface and cycling system. This architecture implies that FLAC3D and PFC3D can be simultaneously loaded into the same graphical user interface and cycled, creating a continuum and allowing DEM model components to coexist within one instance of PFC3D.

The built-in Rblock unit of PFC3D was used to generate the coal seam, immediate, and basic roof. The total thickness of the immediate roof is 5.3 m. According to the prediction method for the fractured zone height in the "coal pillar setting and coal mining regulations for buildings, water bodies, railways, and main roadways [22]," when the mining height is 1.5 m, the fractured zone height in the soft overlying strata is 11.5–19.5 m. Therefore, the total thickness of the basic roof was determined to be 13.0 m. The block model is shown in Figure 4(b). This paper only simulates the influence of mining C_{19} on roof strata movement. Simultaneously, the

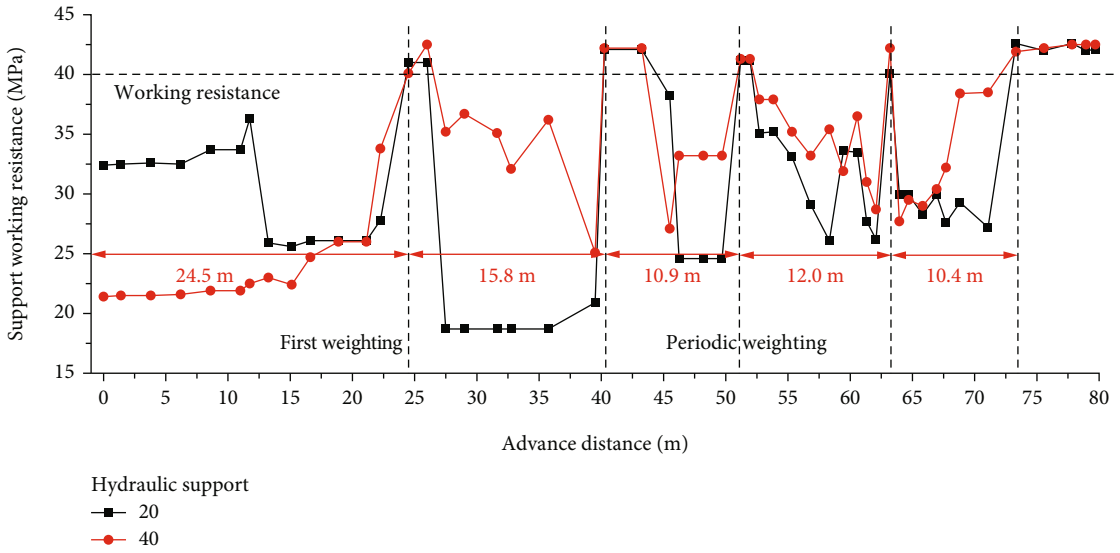

Figure 3: Variation characteristics of support working resistance.

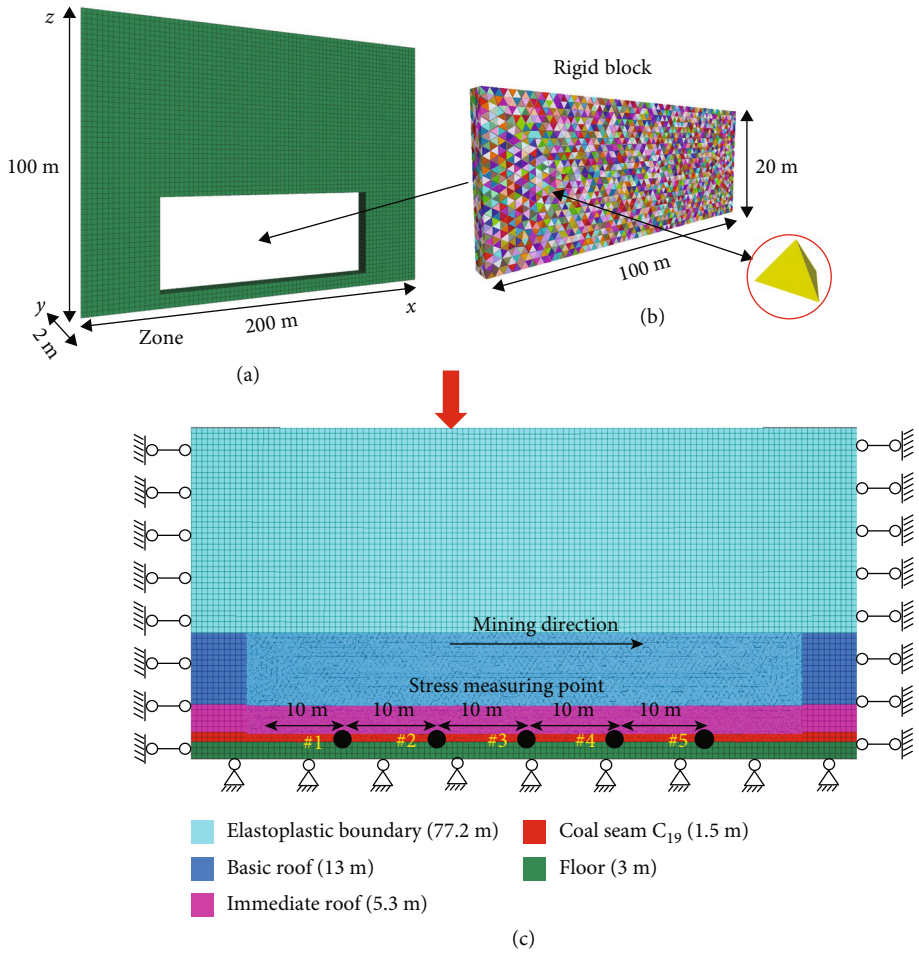

Figure 4: Zone–Rblock coupling model: (a) FLAC3D model, (b) PFC3D, and (c) coupling model.

elastoplastic boundary was simulated using the zone element generated by FLAC3D, as shown in Figure 4(a). The transfer of force and displacement was realized by connecting two different elements through the wall element. The wall zone coupling scheme has been presented in the literature [14, 16, 23].

Table 1: Physical and mechanical parameters of rock strata in the zone [24].

No.	Rock strata	h (m)	ρ (kg/m^3)	E (GPa)	c (MPa)	ψ (°)	σ_t (MPa)	ν
1	Elastoplastic boundary	77.2	3080	1.36	6.10	32	4.32	0.23
2	Basic roof	13	2590	1.72	6.82	39	2.15	0.16
3	Immediate roof	5.3	3020	1.52	6.94	39	3.25	0.20
4	Coal seam C_{19}	1.5	1500	0.05	1.87	42	0.65	0.25
5	Floor	3	2960	1.47	6.94	39	3.15	0.21

Table 2: Mesoscopic particle parameters [21, 25].

Group	Parameter	Symbol	Value
Geometric parameter	Particle maximum-edge (m)	$L_{\max}$	1.0
	Particle minimum-edge (m)	$L_{\min}$	0.5
Constitutive parameters	Particle effective modulus (GPa)	E^*	1.2
	Particle stiffness ratio (–)	k^*	1.0
	Particle friction coefficient (–)	μ	0.577
	Parallel-bond effective modulus (GPa)	$\bar{E}^*$	1.2
	Parallel-bond stiffness ratio (–)	$\bar{k}^*$	1.0
	Parallel-bond tensile strength (MPa)	$\bar{\sigma}_c$	1.5
	Parallel-bond cohesion (MPa)	$\bar{c}$	1.5
	Parallel-bond friction angle (°)	$\bar{\phi}$	30
	Normal critical damping ratio (–)	β_n	0.5

The PFC3D–FLAC3D coupling model is established as follows:

(1) In the PFC3D, a zone element model of FLAC3D with dimensions of $200 \times 100 \times 3$ m was generated, and the strata parameters are listed in Table 1. The equilibrium was calculated under the corresponding boundary and gravity conditions

(2) The displacement of the zone model was initialized to zero, and the 50 m boundary coal pillars were retained on both sides. The zones of the coal seam, immediate roof, and basic roof were deleted for Rblock modeling (Figure 4(a))

(3) The wall zone coupling interface was generated with coincident zone faces composed of edge-connected triangular faces, where vertex velocities and positions were specified as a function of time. A wall plane was established on both sides of the model to limit the y-displacement of the Rblock

(4) The Rblock element was used to generate the coal seam, immediate roof, and basic roof (Figure 4(b)). The numerical model generated by the Rblock elements is called a multi-jointed rock mass model. Based on the mesoscopic parameters of the particles listed in Table 2, they were assigned and iteratively calculated to transfer the self-weight stress of the overlying strata

(5) At 10 m from the open-off cut, five measurement spheres were arranged every 10 m to record the vertical stress, porosity, and particle coordination number variation

(6) Coal seam excavation and data analysis

2.3. Contact Model and Constitutive Parameters. In PFC, the force and displacement are transmitted by the contact between blocks; its generation and fracture law is the contact model. Potyondy and Cundall [26] proposed a contact model that can simulate the mechanical behavior of rocks (i.e., linear parallel-bond model) to reproduce their elasticity, fracture, acoustic emission, and postpeak softening. The contact model provides a force–displacement law for particles, linking the internal force and relative motion between contacts. When the particle gap is ≤0, the contact model is activated, and the force–displacement law for the linear parallel-bond model updates the contact force F_c and moment M_c.

$$\begin{aligned} F_c &= F_l + F_d + \bar{F}, \\ M_c &= \bar{M}, \end{aligned} \tag{1}$$

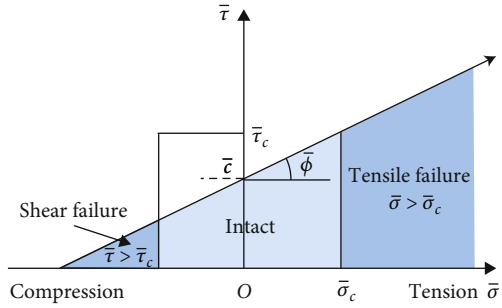

Figure 5: Failure envelope of the linear parallel-bond model.

where F_l is the linear force, F_d the dashpot force, $\bar{F}$ the parallel-bond force, and $\bar{M}$ the parallel-bond moment.

The coal and rock mass are in a three-dimensional compression state under in-situ stress. After the coal-seam mining operation, the vertical stress of the roof decreases, resulting in a contact stress state from compression to tension. The maximum tensile stress $\bar{\sigma}$ and shear stress $\bar{\tau}$ are expressed as follows:

$$\begin{aligned} \bar{\sigma}_{\max} &= \frac{\overline{F_n}}{\bar{A}} + \bar{\beta}\frac{\left|\bar{M}_b\right|}{\bar{I}}\bar{R}, \\ \bar{\tau}_{\max} &= \frac{\overline{F_s}}{\bar{A}} + \bar{\beta}\frac{\left|\overline{M_t}\right|}{\bar{J}}\bar{R}, \end{aligned} \tag{2}$$

where $\overline{F_n}$ and $\overline{F_s}$ are the components of the parallel-bond force in the normal and shear directions, respectively; $\overline{M_b}$ and $\overline{M_t}$ are the parallel-bond bending moment and twist moment, respectively; $\bar{A}$ is the bond cross-section ($A = \pi\bar{R}^2$); $\bar{\beta}$ is the moment-contribution factor ($\bar{\beta} \in [0, 1]$); $\bar{I}$ and $\bar{J}$ are the polar and inertia moments of the bond cross-section ($\bar{I} = 0.25\pi\bar{R}^4$ and $\bar{J} = 0.5\pi\bar{R}^4$); and $\bar{R}$ is the particle radius.

When the roof strata are in the tensile stress state, the following formula can be used to determine whether the parallel-bond breaks:

$$\begin{aligned} &\bar{\sigma} > \overline{\sigma_c}, \\ &\bar{\tau} > \overline{\tau_c} = \bar{c} - \sigma \tan \bar{\phi}, \end{aligned} \tag{3}$$

where $\overline{\sigma_c}$ and $\overline{\tau_c}$ are the parallel-bond tensile and shear strengths, respectively, and $\sigma = \bar{F}_n/\bar{A}$ is the average normal stress acting on the parallel-bond cross-section.

First, the tensile strength criterion is applied during cycling. If $\bar{\sigma} > \overline{\sigma_c}$, then parallel-bond tensile failure occurs; if $\bar{\sigma} \le \overline{\sigma_c}$, then the shear strength criterion is applied; if $\bar{\tau} > \overline{\tau_c}$, then shear failure occurs in the parallel bond. The failure envelope of the parallel-bond model is shown in Figure 5.

The physical and mechanical parameters of the coal and rock strata were obtained through laboratory tests. The parameters were then calibrated according to the measured convergence between the roof and floor of the roadway. The calibration results for the zone model parameters are listed in Table 1. Directly measuring the mesoscopic parameters of Rblocks in the laboratory is difficult. Yuan et al. [21] studied the macromeso parameters of the goaf material in Weixin coal mine, a neighboring mine with Xuyong No.1 coal mine and referenced in this study. The trial and error method was used to adjust the caving effect of the immediate roof. The mesoscopic parameters of calibrated particles are shown in Table 2. The linear parallel-bond model was chosen as the contact model between the particles, whereas the linear contact-bond model was selected as the contact model between the particles and wall [26].

2.4. Roof Movement Characteristics. Figure 6 shows the collapse and accumulation characteristics of the immediate roof after an advance of 5 m along the strike of the working face. As shown in Figure 6(b), after the separation of the immediate roof, the rock blocks with a low bond strength first separated from the rock mass and sank under self-weight to form an irregular caved zone. The initial accumulation height of the caved zone was 2.0 m (Figure 6(c)). Subsequently, owing to the adjustment of the spatial position of the rock block, the shape of the caved zone gradually changed. The accumulation shape is concave (Figure 6(d)). The rock block maximum displacement of the caved zone was 2.0 m, which was greater than the mining height of 1.5 m, indicating that horizontal extrusion and movement occurred on the floor. The fracture height of the immediate roof was 1.0 m, the final accumulation height of the caved zone was 1.5 m, and the bulking factor was 1.5.

Figure 7 shows the movement characteristics of the rock blocks. As shown in Figure 7(a), the rock blocks moved downward at an initial velocity of zero after being separated from the immediate roof, and the velocity increased continuously under the action of gravity. When the rock blocks contacted the floor, the velocity decreased immediately and the peak velocity varied from rock to rock. The particle trajectory was not entirely along the direction of gravity and the rock blocks moved horizontally after contacting the floor. For example, particle 5501 moved 0.3 m in the y-direction (Figure 7(b)). After contact between the rock block and the floor, the movement along the horizontal direction belonged to the stress adjustment process inside the caved zone.

Figure 8 shows the fracture and movement characteristics of the overlying strata. As shown in the figure, the internal structural plane of the rock mass generated by the Rblock tetrahedral element was highly developed, effectively reproducing the development of sandy mudstone joints. The immediate roof was divided into five strata, the basic roof into six strata, and the simulated coal seam was excavated 5 m each time. It can be seen from the figure that when the advancing length of the working face is 10 m (Figure 8(a)), immediate roof 1 partially caved and filled the goaf, the caving height was 1.0 m, and the maximum height of the caved zone was 1.5 m, and bulking factor was 1.5. At this instant, there was no apparent separation of overlying strata. When the advancing length of the working face was 20 m (Figure 8(b)), immediate roof 1 completely caved and filled the goaf, forming an irregular caved zone, and the caving height increased to 2.3 m. Immediate roofs 2, 3, and 4 were broken in the form of rock beams, forming a regular caved zone, and producing obvious separation fissures. The roof

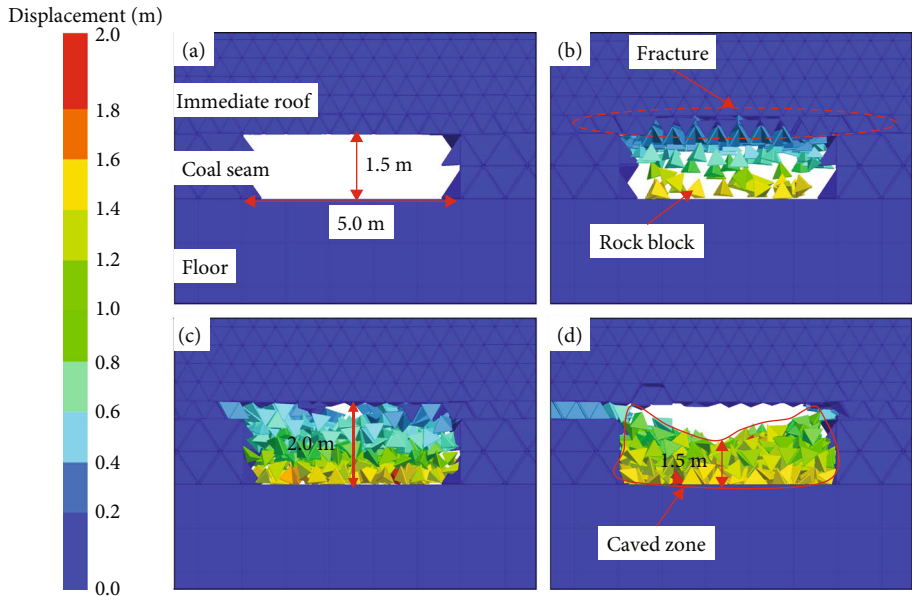

Figure 6: Immediate roof separation, collapse, and accumulation characteristics: (a) coal seam mining, (b) separation, (c) collapse and accumulation, and (d) volume shrinkage of caved zone.

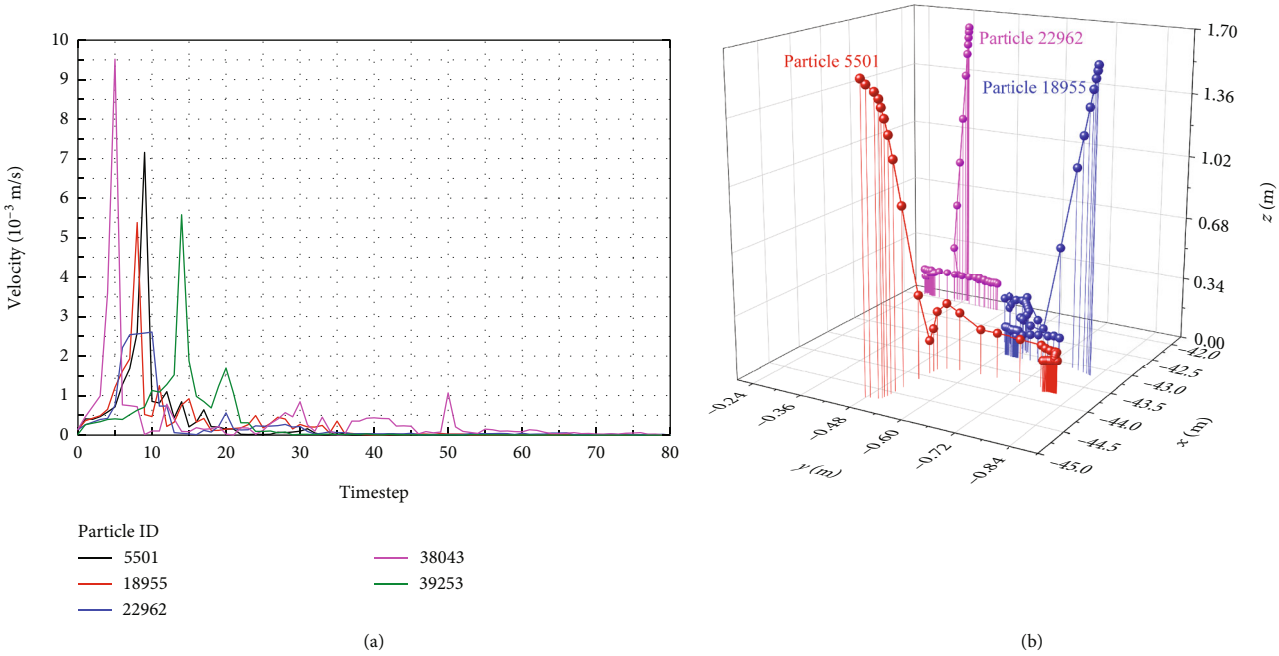

Figure 7: Rock particle movement characteristics.

fracture line was located above the coal wall, and the height of the fractured zone increased to 4.4 m. When the advancing length of the working face was 30 m (Figure 8(c)), immediate roofs 1 and 2 caved and filled the goaf, and the height of the caved zone was further increased to 4.1 m. Immediate roofs 3, 4, and 5 slipped along the coal wall. Basic roofs 1, 2, and 3 fractured, producing separation fissures. When the advancing length of the working face was 50 m (Figure 8(d)), the immediate roof shear slipped along the coal wall, and the basic roof exhibited continuous subsidence without apparent separation.

Considering the above analysis, when the structural plane of the overlying strata is highly developed, the basic roof is characterized by beam fracture only during the initial mining period (the advancing length of the working face is less than 30 m). Immediate roof 1 caved and formed an irregular caved zone, whereas immediate roofs 2, 3, and 4 fractured in the form of rock beams and formed regular

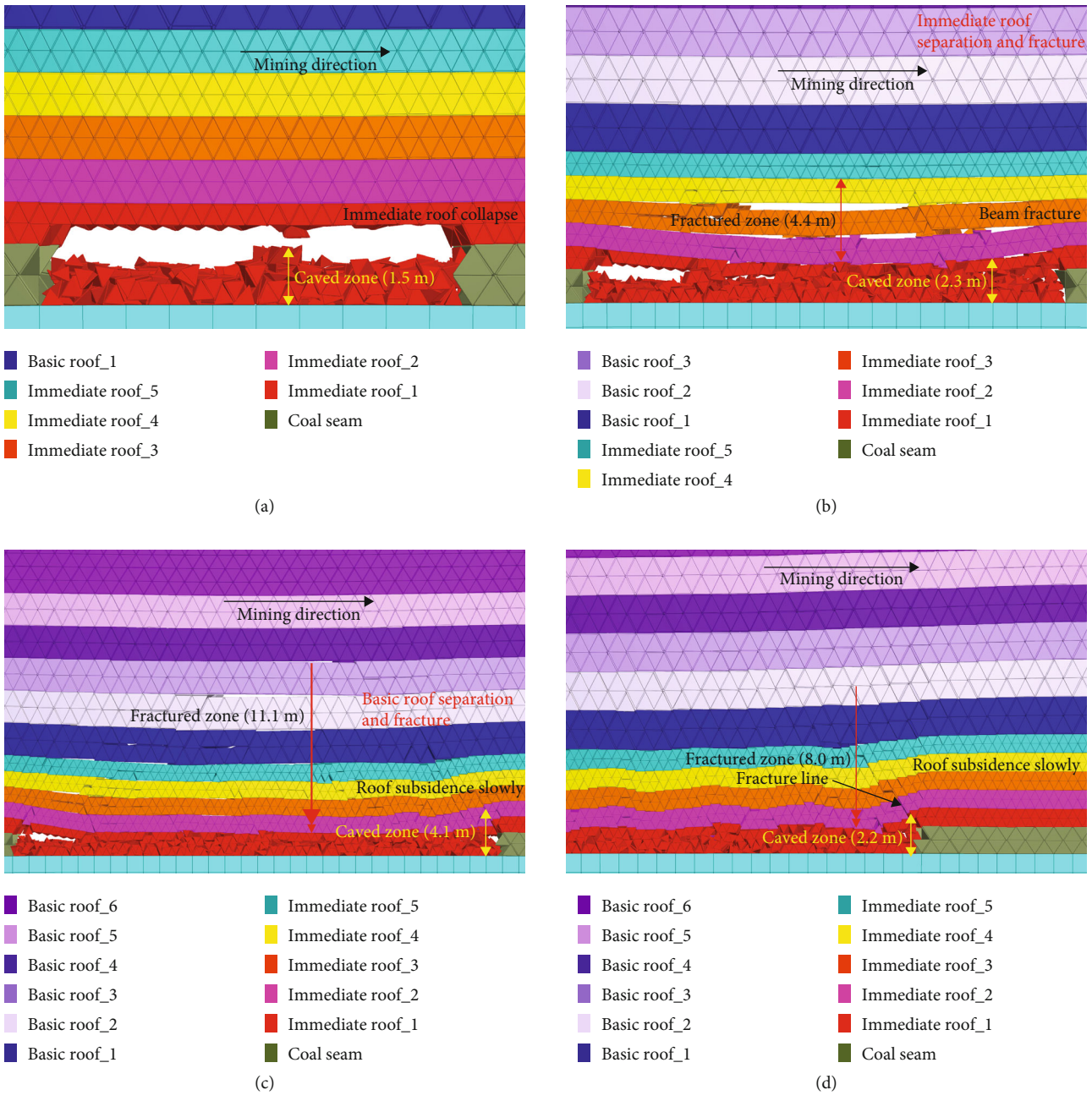

Figure 8: Roof collapse and movement characteristics.

caved zones. After the normal advance of the working face (the advancing length of the working face was greater than 30 m), the immediate roof shear slipped along the coal wall, and the movement of the roof exhibited continuous subsidence. The basic roof fracture does not form a voussoir beam structure, with no apparent separation between the immediate and basic roofs. The shear slip of the immediate roof explained the roof cutting and support crushing of the working face under the soft and multijointed rock mass.

Statistics showing the development laws of the two zones under different advancing lengths are shown in Figure 9. According to the empirical formula [27], when the mining height is 1.5 m, the caved and fractured zone heights are 2.1–5.1 m and 11.5–19.5 m, respectively. From Figure 9, when the advancing lengths of the working face were 10, 20, 30, and 50 m, the maximum height of the caved zone was 1.5, 2.3, 4.1, and 2.2 m, respectively, indicating that the maximum development height of the caved zone increased with advancement for displacements less than 30 m. When the advancing length was greater than 30 m, owing to the fracture subsidence of the basic roof (Figure 8(c)), the caved zone gradually recompacted, and the volume shrank. The final 2.2-m height of the caved zone was consistent with the empirical calculation results.

The fractured zone heights corresponding to the advancing lengths of the working face were 0.0, 4.4, 11.1, and 8.0 m, respectively, indicating that the fractured zone height increased with the mining length before 30 m. Figure 8(c)

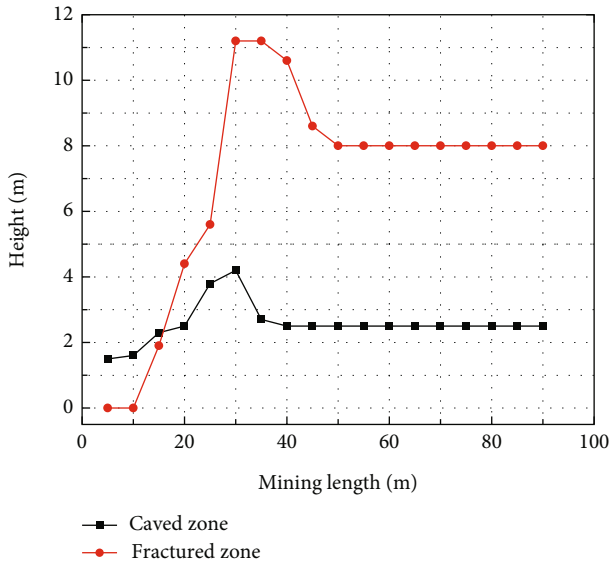

Figure 9: Height of two zones variation law.

shows that when the longwall mining length was 30 m, there was a prominent separation in the rock mass of the fractured zone. When the advancing length was greater than 30 m, the fractures gradually closed and the height decreased to 8.0 m.

2.5. Abutment Pressure Evolution Law. Stress is a continuous quantity; therefore, it does not exist at any point in a particle assembly because the medium is discrete. In the discrete PFC3D model, the contact forces and particle displacements were computed. These quantities help study material behavior on a microscale; however, they cannot be directly transferred to a continuum model. Averaging procedures are necessary to transfer from the microscale to a continuous model. The average stress $\bar{\sigma}_{ij}$ in the measurement region of volume V is computed as

$$\bar{\sigma}_{ij} = -\frac{1}{V}\sum_{N_c} F^{\mathrm{AB}} L^{\mathrm{AB}}, \tag{4}$$

where N_c is the number of contacts in the measurement region or on its boundary, F^{AB} is the contact force vector, and L^{AB} is the branch vector that joins the centroids of two bodies in contact.

Figure 10 shows the variation law of the abutment pressure at measuring point #3 before and after the coal excavation. The coordinate origin and positive and negative axes represent the working face's coal wall, front, and back. The figure shows that the variation of abutment pressure can be divided into four stages according to its spatial relationship with the working face: the front abutment pressure-appearing and pressure-concentration zones and the back abutment pressure-rising and pressure-stable zones. When the point was 30 m from the open-off cut, the front abutment pressure increased gradually, and the coal and rock mass were in the front abutment pressure-appearing zone. When the working face was 10 m from the point, the abutment pressure increased, making this stage the front abutment pressure concentration zone. The abutment pressure peak was 5.7 MPa and the stress concentration coefficient was 1.74. After the working face excavated point #3, the abutment pressure dropped to zero, and it did not change significantly in the 5-m range behind the working face. However, it increased again when the point was 5 m behind the working face, thereby compacting the caved zone. The variation law of the abutment pressure is consistent with the results of Mukherjee et al. [28, 29]. After the goaf was 53.1 m away from the working face, the abutment pressure gradually stabilized, and the stable stress was 3.2 MPa, indicating that the roof activity was stable after mining up to 54 m, and the goaf entered the stable state.

The abutment pressure distribution of the in-situ rock mass was disturbed by coal seam mining, a stress concentration area formed in front of the working face, and a stress reduction area in the rear. After the basic roof is fractured, the weight of the overlying strata acts on the caved zone, causing the goaf abutment pressure to recover gradually [29]. Figure 11 shows the redistribution characteristics of the abutment pressure when the advancement of the working face was 30, 60, and 90 m. The positive and negative axes represent the front and rear of the working face, respectively. The figure shows that the front abutment pressure decreased with fluctuation, which was the reason for the discontinuity of the Rblock. The abutment pressure of the goaf has a jumping and discontinuous distribution, which is different from the results obtained using the continuum medium method [30] and Yavuz's [29] research conclusions (Figure 11(d)). The abutment pressure on the goaf was high in the middle and low on both sides. The stress concentration area was located in the middle of the goaf owing to the discontinuous and irregular accumulation of rock blocks, concentrating stress in the local blocks after roof weighting. When the advancing length of the working face was 30 m (Figure 11(a)), the abutment pressure of the goaf was smaller than that of the in-situ stress; the peak value of the abutment pressure was 1.6 MPa, and the average stress was 0.22 MPa. When the advancing length of the working face was 60 m (Figure 11(b)), the peak value of the abutment pressure increased to 5.6 MPa, which exceeded the in-situ stress of 3.5 MPa. The stress concentration coefficient was 1.6, and the average stress was 0.57 MPa. When the advancing length of the working face was 90 m (Figure 11(c)), the peak value of the abutment pressure increased to 7.8 MPa, the stress concentration coefficient was 2.2, and the average stress increased to 0.96 MPa.

Considering the above analysis, using the multijointed rock mass model generated by the Rblock, the fluctuation in the front abutment pressure of the working face decreases, and the goaf exhibits a jumping and discontinuous pressure distribution. The abutment pressure on the goaf was high in the middle and low on both sides. The block stress concentration area is in the middle of the goaf, and the average abutment pressure increases with the advancing length. The above analysis indicates that the model generated by the Rblock reflects the heterogeneity of coal and rock mass and the discrete characteristics of the rock mass in the caved and fractured zones, which is more realistic than other numerical simulation methods.

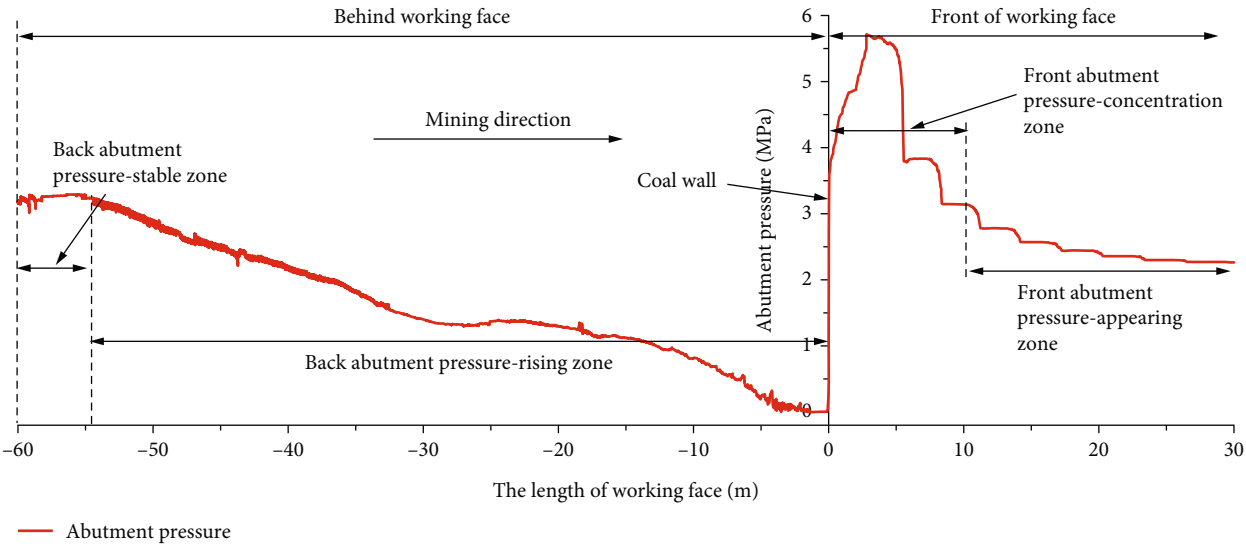

Figure 10: Variation law of abutment pressure of point #3.

2.6. Goaf Material Meso-Parameter Variation Characteristics

2.6.1. Porosity. The porosity n is defined as the ratio of the total void volume V^{void} within the measurement region to the measurement-region volume V^{reg}

$$n = \frac{V^{\text{void}}}{V^{\text{reg}}} = \frac{V^{\text{reg}} - V^{\text{mat}}}{V^{\text{reg}}} = 1 - \frac{V^{\text{mat}}}{V^{\text{reg}}}, \tag{5}$$

where V^{mat} is the volume of material in the measurement region.

Figure 12 shows the various characteristics of the porosity in the goaf. After coal seam mining, the porosity decreases from 0.96, with the descent range becoming smaller when the measuring point lagged behind the working face for a distance. Porosity is closely related to the compaction state of the goaf. In the initial accumulation state, the caved zone was loose and had a large porosity. The mined-out area was compressed by continuum roof subsidence, resulting in a decrease in porosity. When the variation was slight, the volume of the goaf did not change, the relative position of the rock block remained stable, and the goaf reached a relatively steady state. It is evident from the diagram that, after the measuring point lagged behind the average 53.1 m of the working face, the variation in porosity decreased gradually, indicating that the goaf entered a steady state. The porosity at each measuring point differed, and the average porosity was 0.437 after stabilization.

2.6.2. Coordination Number. The coordination number, C_n, is defined as the average number of active contacts per Rblock and is computed as

$$C_n = \frac{\sum_{N_b} n_c^{(b)}}{N_b}, \tag{6}$$

where the summation is taken over N_b Rblocks with centroids in the measurement region, and $n_c^{(b)}$ is the number of active contacts of Rblock b.

Figure 13 shows the variation in the particle coordination number with the advancing length of the working face. The particle coordination number refers to the average number of contacts between a single particle and others. The particle coordination number also reflects the degree of compaction in the caved zone. It can be seen from the figure that the average initial coordination number was 6.8 under in-situ stress. The particle coordination number remained unchanged when the working face was far from the measuring point. When the working face was approximately 5–10 m from the measuring point, the coordination number increased gradually, reaching a peak value at 5 m, and then declined. After coal seam mining, the coordination number decreased to zero, causing the immediate roof to collapse and accumulate in the goaf. The coordination number increases gradually and tends to be stable after the measuring point lagged behind an average working face of 53.1 m. The coordination number's goaf steady distance was the same as the porosity. The average coordination number was 5.9 after stabilization.

3. Similar Simulation Test

A similar simulation test was used to analyze the fracture characteristics of the roof and the variation law of abutment pressure after coal seam mining. Based on the similarity principle [31], similar ratios of physical quantities are defined as follows: geometric ratio, $C_l = l_p/l_m$; volumetric weight ratio, $C_\gamma = \gamma_p/\gamma_m$; displacement ratio, $C_\delta = \delta_p/\delta_m$; strain ratio, $C_\varepsilon = \varepsilon_p/\varepsilon_m$; Poisson ratio, $C_\mu = \mu_p/\mu_m$; stress ratio, $C_\sigma = \sigma_p/\sigma_m$; elastic modulus ratio, $C_E = E_p/E_m$; cohesion ratio, $C_H = H_p/H_m$; internal friction angle ratio, $C_I =$

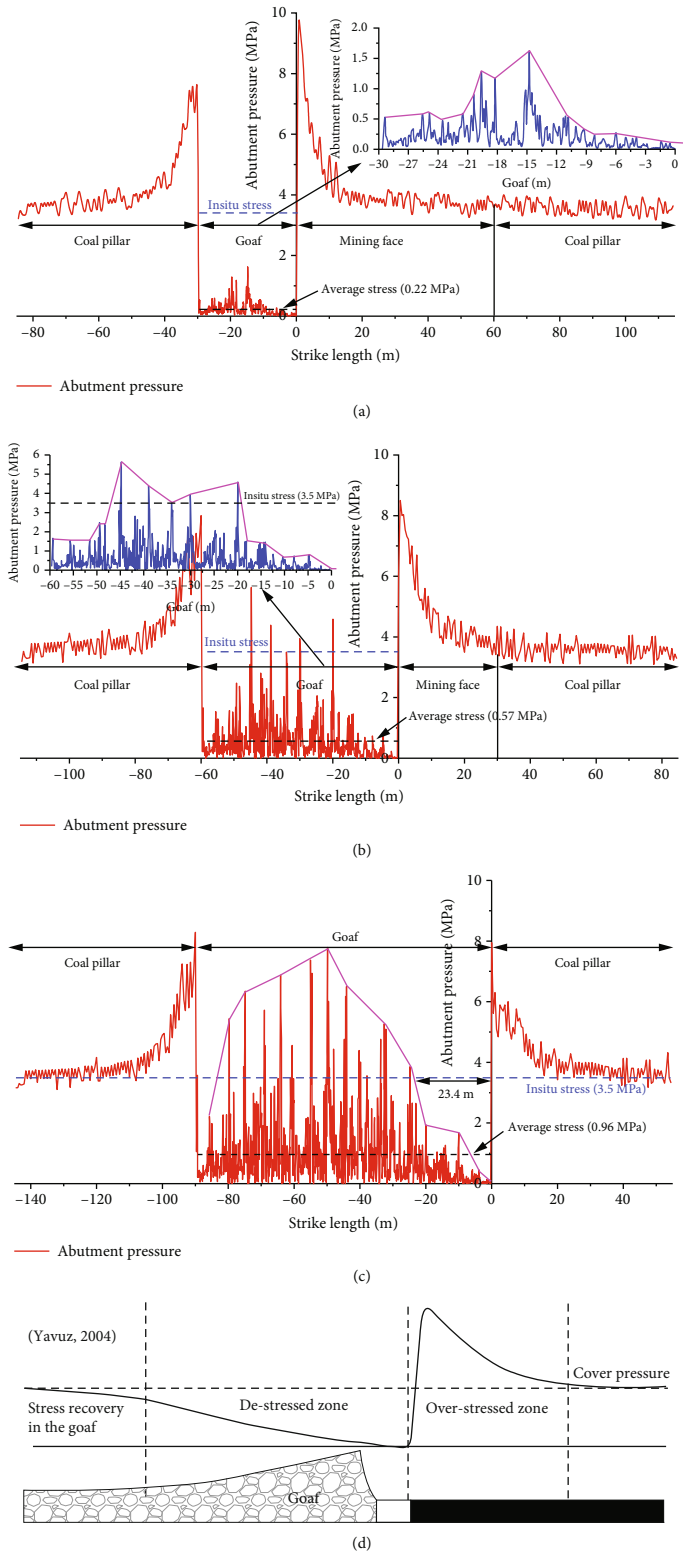

Figure 11: Abutment pressure redistribution characteristics.

I_p/I_m; and time ratio, $C_t = t_p/t_m$. The essential similarity criteria were $C_\sigma = C_l C_\gamma$, $C_E = C_\sigma$, $C_\delta = C_l$, $C_t = \sqrt{C_l}$, and $C_\varepsilon = C_\mu = C_I = 1$. In addition, the stress similarity ratio must be consistent; that is, $C_\sigma = C_E = C_{\sigma_c} = C_{\sigma_t} = C_H$. p and m represent the physical quantities of the prototype and model, respectively; C denotes a similar ratio.

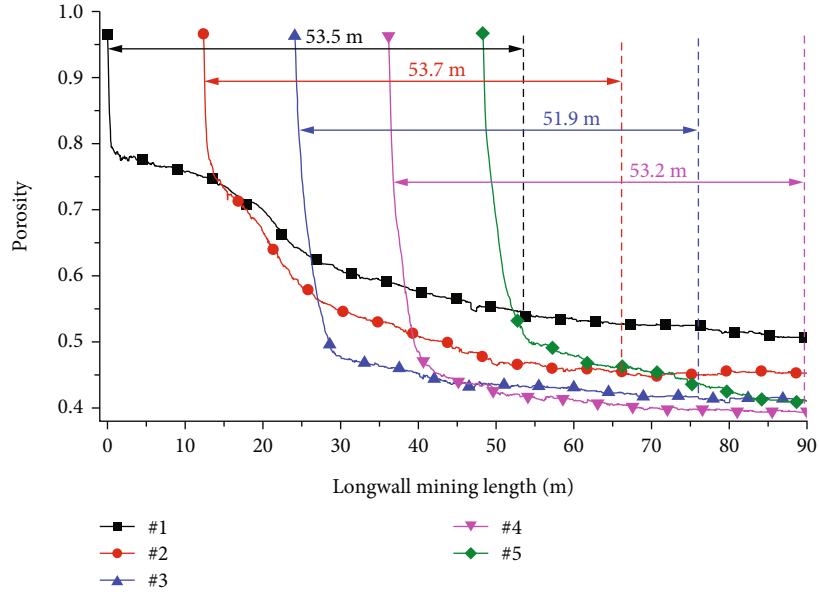

Figure 12: Porosity variation characteristics.

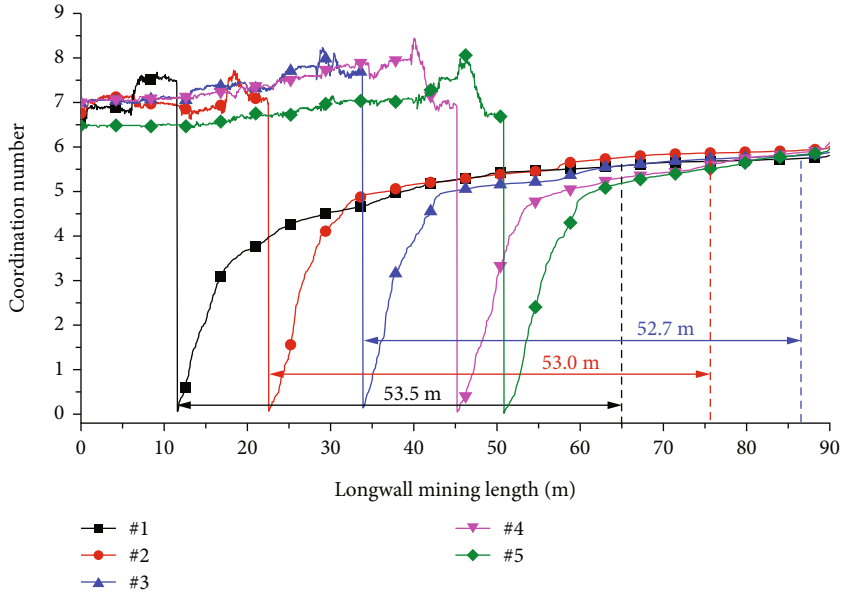

Figure 13: Variation characteristics of particle coordination number.

The geometric similarity ratio is typically between 1 : 20 and 1 : 400. Considering the low mining height of the working face, the selection of the geometric ratio should be maximum; however, an excessive ratio limits the advancing length of the working face. Therefore, the geometrically similar ratio of the model was determined as 1 : 50. The volumetric weight ratio is usually 1 : 1.6, and the stress and time similarity ratios were calculated from $C_\sigma = C_l C_\gamma$ and $C_t = \sqrt{C_l}$. The main similar constants were determined as listed in Table 3.

Table 3: Similar constants.

Physical quantity	Symbol	Similar ratio
Geometric ratio	C_l	1 : 50
Volumetric weight ratio	C_γ	1 : 1.6
Stress ratio	C_σ	1 : 80
Time ratio	C_t	1 : 7

3.1. Materials and Equipment. Accurate coal seam excavation is an important factor affecting similar simulation results, and there has always been over- or under-excavation using the cutting method. Therefore, this test used the woodblock extraction method to quickly and accurately simulate coal seam mining. Woodblocks with sizes of

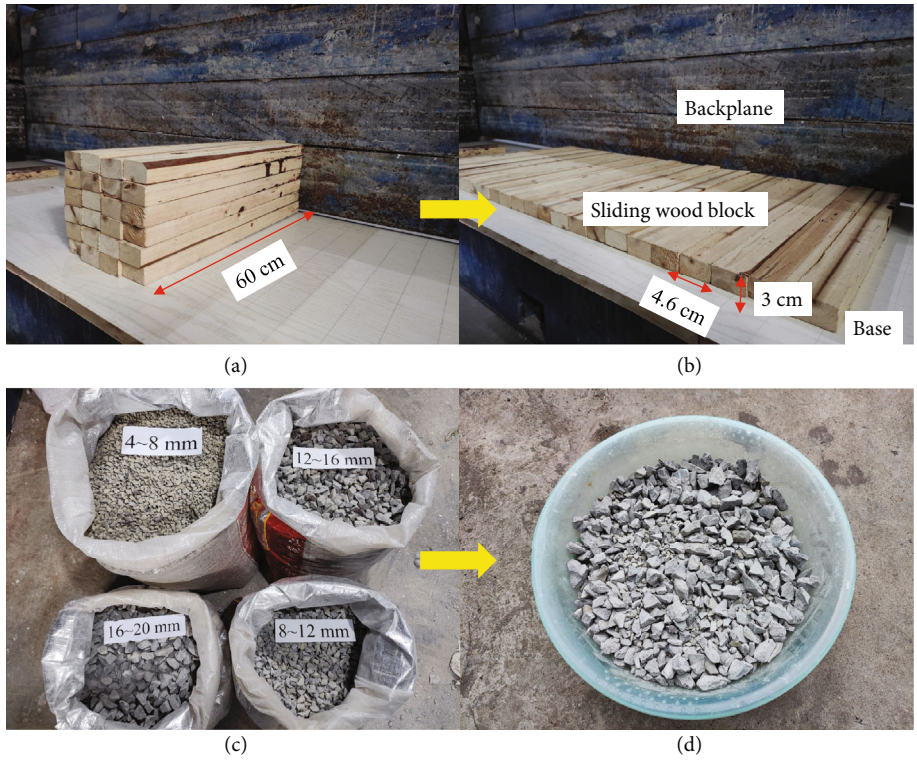

FIGURE 14: Similar material of coal seam and immediate roof: (a) woodblock, (b) similar material of coal seam, (c) single-gradation rock particles, and (d) mixed particle size gradation.

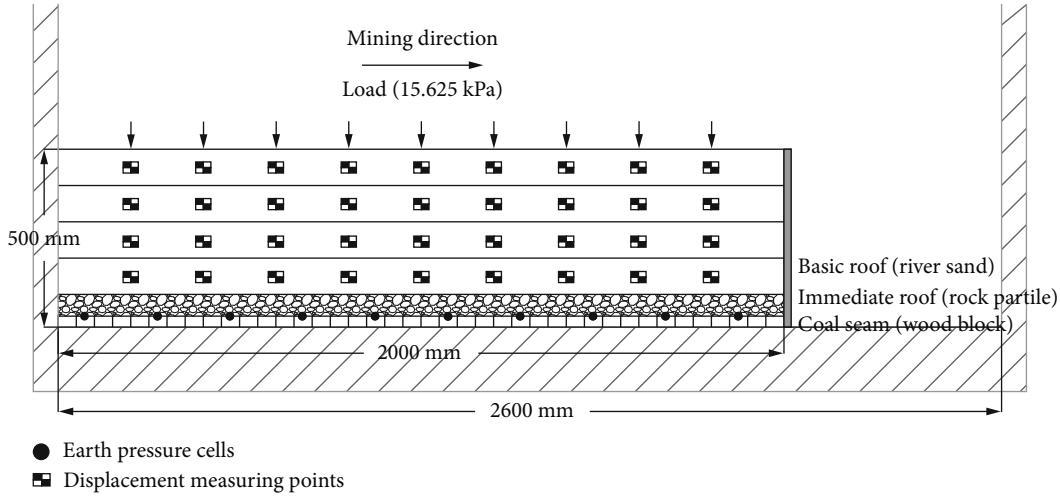

FIGURE 15: Physical model diagram.

$60 \times 4.6 \times 3$ cm were arranged in an orderly manner as coal seam similar materials, as shown in Figures 14(a) and 14(b), and the mining height was 1.5 m. The woodblocks were individually drawn backward during coal seam mining.

The immediate roof fractures and collapses after coal excavation. Most similar simulation tests [32, 33] have shown a plate-shaped fracture in the immediate roof. In comparison, in the field, the immediate roof fractured and formed a block shape (Figure 1). Therefore, the material properties of the immediate roof significantly influence the shape characteristics of the caved zone, and its compression and deformation characteristics affect the fracture and subsidence of the basic roof. According to the shape characteristics of rock blocks in the field-caved zone, a physical model filled rock particles in the immediate roof to simulate rock blocks of different sizes and shapes formed in the goaf after the collapse of the immediate roof (Figures 14(c) and 14(d)). A diagram of the physical model is shown in Figure 15.

The rock particle size gradations of the simulated goaf were 0.2 – 0.4, 0.4 – 0.6, 0.6 – 0.8, and 0.8 – 1.0 m. The particle

Table 4: Model strength and material proportion number.

Strata	Lithology	Model thickness (cm)	Proportion number	σ_t (MPa)	
				Prototype	Model
Basic roof	Sandy mudstone	30	437	2.15	0.027

Note: the first digit of the proportion number represents the sand-cement ratio, and the second and third digits represent the proportions of lime and gypsum in one cement, respectively.

Table 5: Similar material consumption in basic roof.

Thickness (cm)	Layer	Density (kg/m^3)	Sand (kg)	Lime (kg)	Gypsum (kg)	Water (kg)	Borax (g)
30	15	1800	270	16.2	37.8	36	360

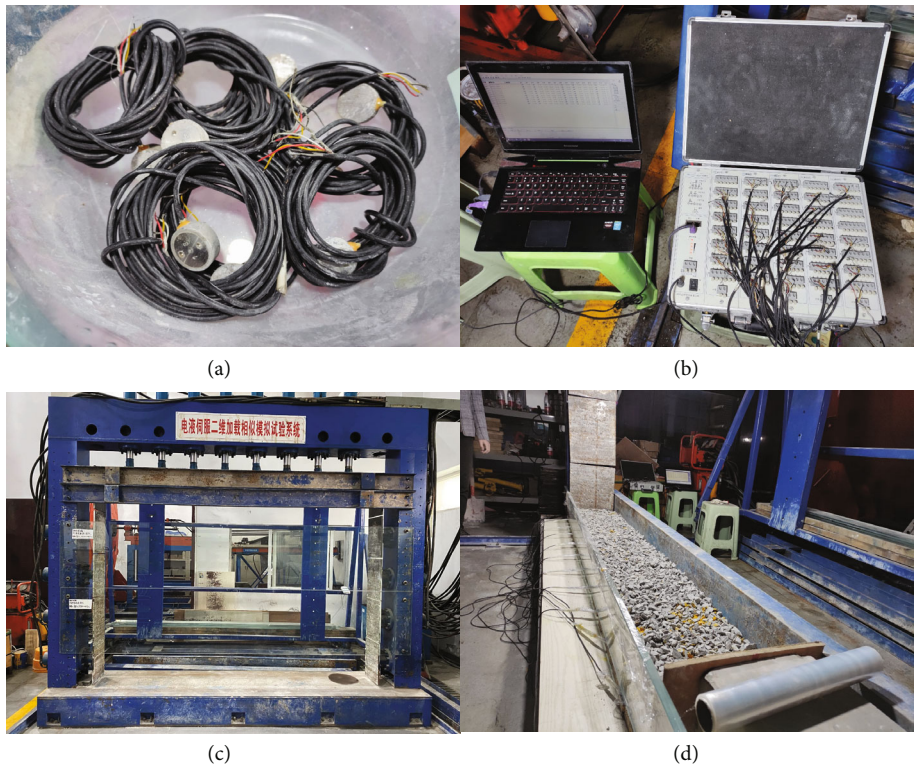

Figure 16: Test equipment: (a) earth pressure cells, (b) JM5951 static strain test system, (c) physical model frame, and (d) rock particles.

size gradations of rock particles converted according to similar geometric ratios were 4 – 8, 8 – 12, 12 – 16, and 16 – 20 mm. Assuming that the rock particle size of the goaf obeyed a normal distribution, the mass fractions of each gradation were 10, 40, 40, and 10%. Therefore, the required masses of the rock particles were 5.38, 21.47, 21.47, and 5.38 kg.

Referring to *the Rock Mechanics Experimental Simulation Technology*, according to the model tensile strength of the basic roof in Table 4, this test used river sand as the aggregate, gypsum as the main cementing material, and lime as auxiliary cementing materials. The proportion was 537. The water content was 1/10 of the mixture, and the model was naturally dried to a moisture content of 8%. The consumption of similar materials are presented in Table 5.

Figure 16 shows the test and stress-monitoring equipment.

The similar simulation test steps are as follows:

(1) Install the front and rear baffles of the model frame

(2) Sliding woodblocks were laid on the base, and earth pressure cells were placed (Figure 16(a)), that were connected to the JM5951 static strain instrument (Figure 16(b)).

(3) The size-mixed rock particles were dyed in three colors (red, yellow, and gray) and layered into the model as the immediate roof (Figure 16(d)).

(4) The river sand was mixed with the cementing materials in Table 5, followed by molding and tamping as the basic roof

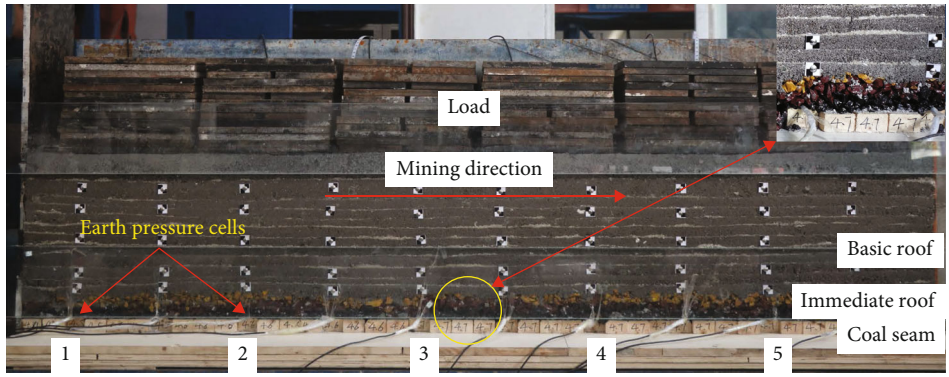

Figure 17: Physical model entity graph.

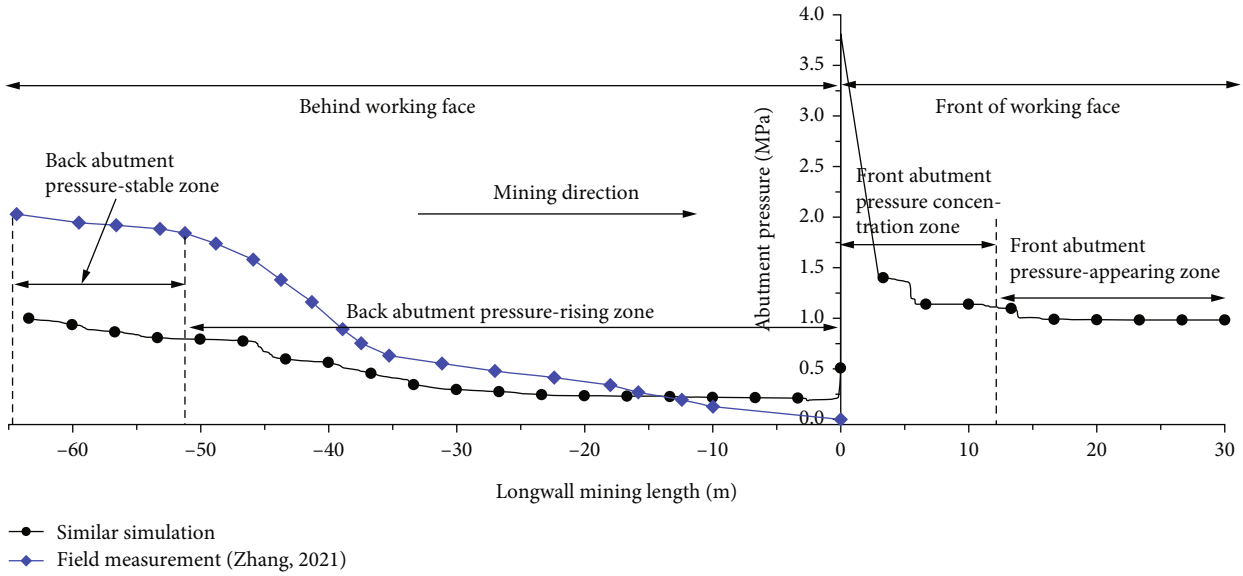

Figure 18: Comparison diagram of abutment pressure variation.

(5) The upper boundary of the model was applied with 15 $30 \times 30 \times 1$ cm iron blocks as the self-weight of the overlying strata, and the simulated overburden depth was 100 m. The physical model with dimensions of 2 m × 0.3 m × 0.5 m is shown in Figure 17

3.2. Test Results. Figure 18 compares the variation law of abutment pressure obtained using different research methods. Here, the stress and length units in similar test results were converted into actual field results based on a similar ratio. From Figures 10 and 18, the variation characteristics of the abutment pressure obtained by the numerical and similar simulations were the same, and the variation law of the abutment pressure in the goaf was the same as that in the field measurement [34]. The numerical and similar simulation results indicated that the variation in abutment pressure could be divided into four stages according to its spatial position relationship with the working face.

Figure 19 shows the variation law of the abutment pressure at different measuring points during the mining process of the working face. As shown in the figure, the variation in abutment pressure at the measuring point exhibited the characteristics of the four stages; however, points No. 1 and No. 5 near the coal pillar boundary had no back abutment pressure-rising zone, indicating that the caved zone near the coal pillar was not recompacted. The peak values of advanced abutment pressure at measuring points 1–5 were 4.7, 3.8, 3.7, 4.9, and 3.9 MPa, respectively.

Figure 20 shows similar simulation results of roof fracture and movement characteristics with working face advancement lengths of 20, 40, 60, and 80 m. The immediate roof collapsed continuously, filled the goaf with the advance of the working face, and exhibited "with mining and caving", similar to the numerical simulation results. When the advancing length of the working face was 20 m (Figure 20(a)), the basic roof was suspended. When the mining length was 25 m, the basic roof was separated, and subsidence and fracture closure occurred. After the advancing length of the working face was greater than 40 m (Figures 20(c) and 20(d)), the basic roof subsided continuously and slowly owing to the support of the goaf materials.

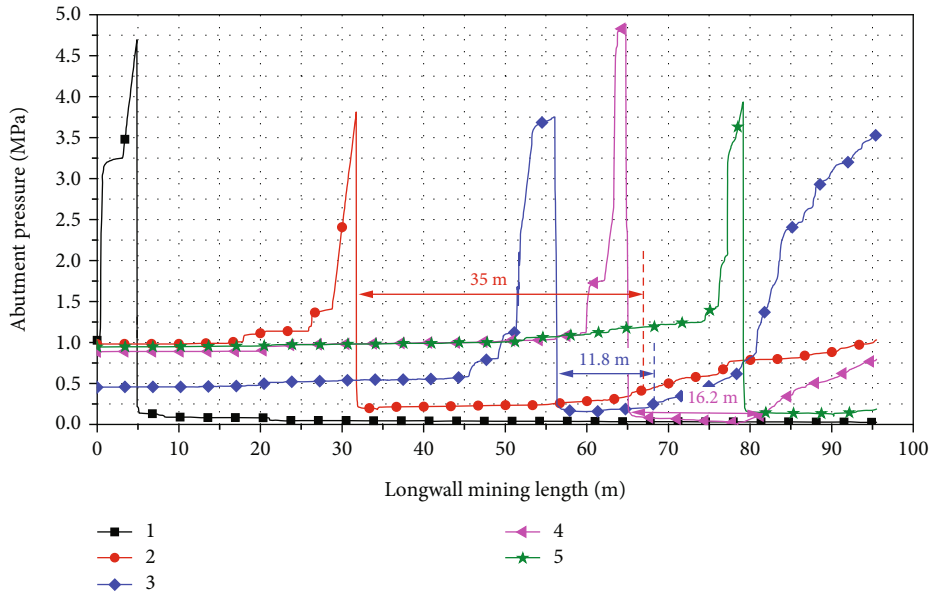

Figure 19: Similar simulation of variation law of abutment pressure.

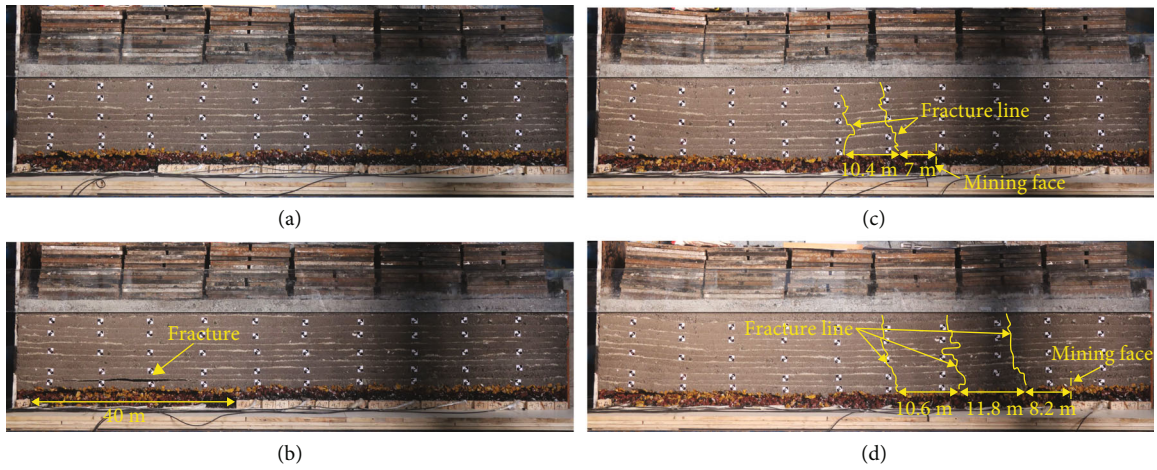

Figure 20: Similar simulation of roof fracture and movement characteristics at longwall mining lengths: (a) 20 m, (b) 40 m, (c) 60 m, and (d) 80 m.

4. Conclusions

(1) The multijointed rock mass model generated by the Rblock element reproduced the development characteristics of soft rock joints. After coal seam mining, the immediate roof caved and filled the goaf, forming irregular and regular caved zones. The maximum development height of the caved zone first increased to 4.1 m with the advancement of the working face, decreased to 2.2 m, and remained unchanged. The shear slip of the immediate roof along the coal wall explains the roof cutting and support crushing at the working face. The fracture of the basic roof formed a fractured zone, and the initial fracture step distance was 25 m. The maximum height of the fracture zone also increased to 11.2 m, decreased to 8.0 m, and remained unchanged. The main roof exhibits continuous slow subsidence

(2) The variation in abutment pressure can be divided into four stages according to its spatial relationship with the working face: front abutment pressure-appearing and pressure-concentration zones and back-abutment pressure-rising and pressure-stable zones. The redistribution characteristics of abutment pressure in the mining face were as follows: the fluctuation of the front abutment pressure was reduced, and the abutment pressure in the goaf jumps is discontinuous. The abutment pressure in the goaf was high in the middle and low on both sides. After the initial fracture of the basic roof, the stress concentration of some rock blocks in the goaf exceeded the in-

situ stress, and the average abutment pressure increased with an increase in the working face advancing length

(3) As the coal wall of the mining face moved away from the goaf, the abutment pressure increased to 3.2 MPa and remained constant. The porosity decreased slowly after a sharp decline to 0.437; the particle coordination number rose sharply to 5.9 and then declined slowly, indicating that the goaf was gradually in a stable state. This conclusion provides a reference for the layout timing of entry in close-distance coal seam groups

(4) Similar simulation results indicated that the variation law of abutment pressure, caving characteristics of the immediate roof, and continuous slow subsidence of the basic roof were the same as those of the numerical simulation. The caving features of the immediate roof in the goaf and the roof-cutting phenomenon in the coal face conformed to the field situation, indicating that it is reasonable and feasible to study the movement law of multijointed overlying strata and abutment pressure distribution. This method provides a new approach for studying the movement laws of multijointed overlying strata and the prevention and control of roof disasters

Data Availability

All data, models, and code generated or used during the study appear in the submitted article.

Conflicts of Interest

The authors declare that they have no known competing financial interests or personal relationships that could have influenced the work reported in this paper.

Acknowledgments

This work was supported by the Xuyong No.1 coal mine of Sichuan Coal Group.

References

[1] C. Zhang, S. H. Tu, and Y. X. Zhao, "Compaction characteristics of the caving zone in a longwall goaf: a review," *Earth Science*, vol. 78, no. 1, 2019.

[2] S. Wang, X. L. Li, and Q. Z. Qin, "Study on surrounding rock control and support stability of ultra-large height mining face," *Energies*, vol. 15, no. 18, p. 6811, 2022.

[3] V. Palchik, "Bulking factors and extents of caved zones in weathered overburden of shallow abandoned underground workings," *International Journal of Rock Mechanics and Mining Sciences*, vol. 79, pp. 227–240, 2015.

[4] Z. Y. Ti, J. Z. Li, M. Wang et al., "Fracture characteristics and zoning model of overburden during longwall mining," *Shock and Vibration*, vol. 2021, Article ID 2857750, 12 pages, 2021.

[5] X. L. Li, S. J. Chen, S. Wang, M. Zhao, and H. Liu, "Study on in situ stress distribution law of the deep mine: taking Linyi mining area as an example," *Advances in Materials Science and Engineering*, vol. 2021, Article ID 5594181, 11 pages, 2021.

[6] A. Yadav, B. Behera, S. K. Sahoo, G. S. P. Singh, and S. K. Sharma, "An approach for numerical modeling of gob compaction process in longwall mining," *Mining, Metallurgy & Exploration*, vol. 37, no. 2, pp. 631–649, 2020.

[7] J. X. Liu, Y. L. Liu, W. X. Li, X. G. Zhang, and C. R. Xin, "Measures to deal roof-shock during tunneling at deep and extra-thick coal," *Arabian Journal of Geosciences*, vol. 12, no. 6, 2019.

[8] R. Wu, J. H. Xu, C. Li, Z. L. Wang, and S. Qin, "Stress distribution of mine roof with the boundary element method," *Engineering Analysis with Boundary Elements*, vol. 50, pp. 39–46, 2015.

[9] Q. Cheng, Y. Shi, and L. Zuo, "Numerical simulation and analysis of surface and surrounding rock failure in deep high-dip coal seam mining," *Geotechnical and Geological Engineering*, vol. 37, no. 5, pp. 4285–4299, 2019.

[10] X. Gao, S. Zhang, Y. Zi, and S. K. Pathan, "Study on optimum layout of roadway in close coal seam," *Arabian Journal of Geosciences*, vol. 13, no. 15, 2020.

[11] B. Indraratna, N. T. Ngo, C. Rujikiatkamjorn, and S. W. Sloan, "Coupled discrete element-finite difference method for analysing the load- deformation behaviour of a single stone column in soft soil," *Computers and Geotechnics*, vol. 63, pp. 267–278, 2015.

[12] N. T. Ngo and T. M. Tung, "Coupled Discrete-Continuum Method for Studying Load-Deformation of a Stone Column Reinforces Rail Track Embankments," *Procedia Engineering*, vol. 142, pp. 139–145, 2016.

[13] W. A. Curtin and R. E. Miller, "Atomistic/continuum coupling in computational materials science," *Modelling and Simulation in Materials Science and Engineering*, vol. 11, no. 3, pp. R33–R68, 2003.

[14] A. Breugnot, S. Lambert, P. Villard, and P. Gotteland, "A discrete/continuous coupled approach for modeling impacts on cellular geostructures," *Rock Mechanics and Rock Engineering*, vol. 49, no. 5, pp. 1831–1848, 2016.

[15] M. Cai, P. K. Kaiser, H. Morioka et al., "FLAC/PFC coupled numerical simulation of AE in large-scale underground excavations," *International Journal of Rock Mechanics and Mining Sciences*, vol. 44, no. 4, pp. 550–564, 2007.

[16] S. P. Xiao and T. Belytschko, "A bridging domain method for coupling continua with molecular dynamics," *Computer Methods in Applied Mechanics and Engineering*, vol. 193, no. 17-20, pp. 1645–1669, 2004.

[17] Z. Li and Q. H. Rao, "Quantitative determination of PFC3D microscopic parameters," *Journal of Central South University*, vol. 28, no. 3, pp. 911–925, 2021.

[18] X. Tan, Z. B. Hu, M. Cao, and C. F. Chen, "3D discrete element simulation of a geotextile-encased stone column under uniaxial compression testing," *Computers and Geotechnics*, vol. 126, p. 103769, 2020.

[19] M. Li, A. L. Li, J. X. Zhang, Y. L. Huang, and J. M. Li, "Effects of particle sizes on compressive deformation and particle breakage of gangue used for coal mine goaf backfill," *Powder Technology*, vol. 360, pp. 493–502, 2020.

[20] J. M. Li, Y. L. Huang, H. Pu et al., "Influence of block shape on macroscopic deformation response and meso-fabric evolution of crushed gangue under the triaxial compression," *Powder Technology*, vol. 384, pp. 112–124, 2021.

[21] F. Yuan, J. X. Tang, Y. L. Wang, C. Li, and L. R. Kong, "Numerical simulation of mechanical characteristics in longwall Goaf materials," *Mining, Metallurgy & Exploration*, vol. 39, no. 2, pp. 557–571, 2022.

[22] W. Q. Zhang, B. Li, G. B. Zhang, and Z. L. Li, "Investigation of water-flow fracture zone height in fully mechanized cave mining beneath thick alluvium," *Geotechnical and Geological Engineering*, vol. 35, no. 4, pp. 1745–1753, 2017.

[23] E. Frangin, P. Marin, and L. Daudeville, "On the use of combined finite/discrete element method for impacted concrete structures," *Journal de Physique IV*, vol. 134, pp. 461–466, 2006.

[24] S. Y. Jiang, G. W. Fan, Q. Z. Li, S. Z. Zhang, and L. Chen, "Effect of mining parameters on surface deformation and coal pillar stability under customized shortwall mining of deep extra-thick coal seams," *Energy Reports*, vol. 7, pp. 2138–2154, 2021.

[25] B. D. Yang, Y. Jiao, and S. T. Lei, "A study on the effects of microparameters on macroproperties for specimens created by bonded particles," *Engineering Computations*, vol. 23, no. 6, pp. 607–631, 2006.

[26] D. O. Potyondy and P. A. Cundall, "A bonded-particle model for rock," *International Journal of Rock Mechanics and Mining Sciences*, vol. 41, no. 8, pp. 1329–1364, 2004.

[27] X. X. Miao, X. M. Cui, J. A. Wang, and J. L. Xu, "The height of fractured water-conducting zone in undermined rock strata," *Engineering Geology*, vol. 120, no. 1-4, pp. 32–39, 2011.

[28] C. Mukherjee, P. R. Sheorey, and K. G. Sharma, "Numerical simulation of caved goaf behaviour in longwall workings," *International Journal of Rock Mechanics and Mining Science and Geomechanics Abstracts*, vol. 31, no. 1, pp. 35–45, 1994.

[29] H. Yavuz, "An estimation method for cover pressure re-establishment distance and pressure distribution in the goaf of longwall coal mines," *International Journal of Rock Mechanics and Mining Sciences*, vol. 41, no. 2, pp. 193–205, 2004.

[30] X. Y. Zhang, Z. J. Wen, J. G. Liu, L. Luo, and B. Sun, "Research on distribution and evolution laws of surrounding rock stress during the island panel mining in multiple complex stope," *Geotechnical and Geological Engineering*, vol. 37, no. 4, pp. 3355–3366, 2019.

[31] E. Szcs, *Similitude and Modelling*, Elsevier Scientific Pub. Co, 1980.

[32] H. Shi, Y. B. Zhang, and L. Tang, "Physical test of fracture development in the overburden strata above the goaf and diffusion process of permeable grout slurry," *Bulletin of Engineering Geology and the Environment*, vol. 80, no. 6, pp. 4791–4802, 2021.

[33] Y. Wu, Z. Huang, X.-Z. Li, and C.-L. Jiang, "Deformation and failure characteristics of overburden under thin bedrock and thick alluvium: a case study in Baodian coal mine," *Geotechnical and Geological Engineering*, vol. 38, no. 5, pp. 5213–5228, 2020.

[34] G. J. Zhang, Q. S. Li, Y. Zhang, and F. Du, "Failure characteristics of roof in working face end based on stress evolution of goaf," *Geomechanics and Geophysics for Geo-Energy and Geo-Resources*, vol. 7, no. 3, 2021.